

Tunable Electronic Properties and Band Alignments of MoSi₂N₄/GaN and MoSi₂N₄/ZnO van der Waals Heterostructures

Jin Quan Ng,¹ Qingyun Wu,¹ L. K. Ang,^{1,*} and Yee Sin Ang^{1,*}

¹*Science, Mathematics and Technology, Singapore University of Technology and Design (SUTD), 8 Somapah Road, Singapore 487372, Singapore*

Van de Waals heterostructures (VDWH) is an emerging strategy to engineer the electronic properties of two-dimensional (2D) material systems. Motivated by the recent discovery of MoSi₂N₄ - a synthetic septuple-layered 2D semiconductor with exceptional mechanical and electronic properties, we investigate the synergy of MoSi₂N₄ with wide band gap (WBG) 2D monolayers of GaN and ZnO using first-principle calculations. We find that MoSi₂N₄/GaN is a direct band gap Type-I VDWH while MoSi₂N₄/ZnO is an indirect band gap Type-II VDWH. Intriguingly, by applying an electric field or mechanical strain along the out-of-plane direction, the band structures of MoSi₂N₄/GaN and MoSi₂N₄/ZnO can be substantially modified, exhibiting rich transitional behaviors, such as the Type-I-to-Type-II band alignment and the direct-to-indirect band gap transitions. These findings reveal the potentials of MoSi₂N₄-based WBG VDWH as a tunable hybrid materials with enormous design flexibility in ultracompact optoelectronic applications.

In recent years, van der Waals heterostructures (VDWHs) have been widely employed for engineering the electronic, optical and photocatalytic properties of two-dimensional (2D) materials [1]. With an appropriate selection of 2D monolayers and stacking order, VDWHs can give rise to myriads of interesting physics, such as strongly interacting artificial heavy fermions [2], and excitonic Bose-Einstein Condensates [3]. VDWHs also offer an avenue to engineer high-quality electrical contacts [4, 5] with exceptionally low contact resistance and significantly suppressed Fermi level pinning effect, thus playing a pivotal role towards the development of practical 2D semiconductor device technology [6, 7].

As such, VDWHs have the ability to enable applications in new devices not available with currently available materials or enhance current devices with new characteristics. One example of which are tunnelling transistors which operate by tunnelling current [8]. Such devices made using VDWHs promise to have subthreshold swings below traditional MOSFET limits and hence have lower off currents and standby power dissipation, thus better suited for low power applications [9]. Another example are better photodetectors with fast switching speed [10] due to narrow channel width, higher responsivity due to built-in electric fields and broad spectral bandwidth [11].

The recent discovery of MoSi₂N₄ and the extended MA₂Z₄ monolayer family reveals an exciting material platform for designing novel 2D material devices. MoSi₂N₄ monolayer is a *synthetic* 2D semiconductor without 3D parent structure and has been synthesized experimentally by passivating MoN₂ monolayer with Si to create a septuple-layered nanosheet composed of a MoN₂ inner layer sandwiched by two Si-N outer layers [12]. Interestingly, the Conduction Band Minimum (CBM) and the Valence Band Maximum (VBM) are concentrated

within the MoN₂ core-layer and the outer Si-N atomic sublayer, hence serving as a built-in protective layer to preserve the conduction channels from the external perturbations [6, 13] and to strongly suppress the adverse Fermi level pinning effect. Quantum transport simulations have also suggested MoSi₂N₄ monolayer to be an exceptional 2D channel material for field-effect transistor applications [14–16]. Beyond pristine monolayer, MoSi₂N₄ has been predicted to be half metallic with N or Si vacancies [17] and excellent optical absorption in visible light range [18] among many other properties, which provide many potential applications in electronics and photonics.

MA₂Z₄-based VDWHs is an emerging area, recent studies include MoSi₂N₄/TMDC [19, 20] and Janus MA₂Z₄-based VDWHs [21, 22]. Unusual properties, such as electric-field and strain tunable Ohmic-to-contact transition, semiconductor-to-metal transition [23], Type-I-to-Type-II band alignment transition and excellent optical absorption around the visible light regime [21], have been predicted in various MA₂Z₄-based VDWHs. Nonetheless, the synergy of MA₂Z₄ monolayer with wide band gap (WBG) semiconductors, such as GaN and ZnO honeycomb monolayer remains largely unexplored thus far. Due to quantum confinement, WBG monolayers are expected to exhibit a larger band gap than the bulk counterparts [24, 25]. WBG semiconductors have been widely explored for optical [26–28] and electronic device applications [29, 30]. WBG semiconductor typically have a band gap of > 2 eV [31], making them excellent for optoelectronic applications [32] due to higher excitonic binding energy that is robust against thermal fluctuations. The wider band gap is also beneficial for devices operating at higher temperatures and higher voltage operation [33–36]. In particular, 2D ZnO has been experimentally synthesised [37] and investigated for photocatalytic [38] and photodetector capabilities [39]. On the other hand, low-cost and easy growing of high quality, transferable 2D GaN is challenging due to the parent compound being

* Authors to whom correspondence should be addressed: ricky_ang@sutd.edu.sg and yeesin_ang@sutd.edu.sg

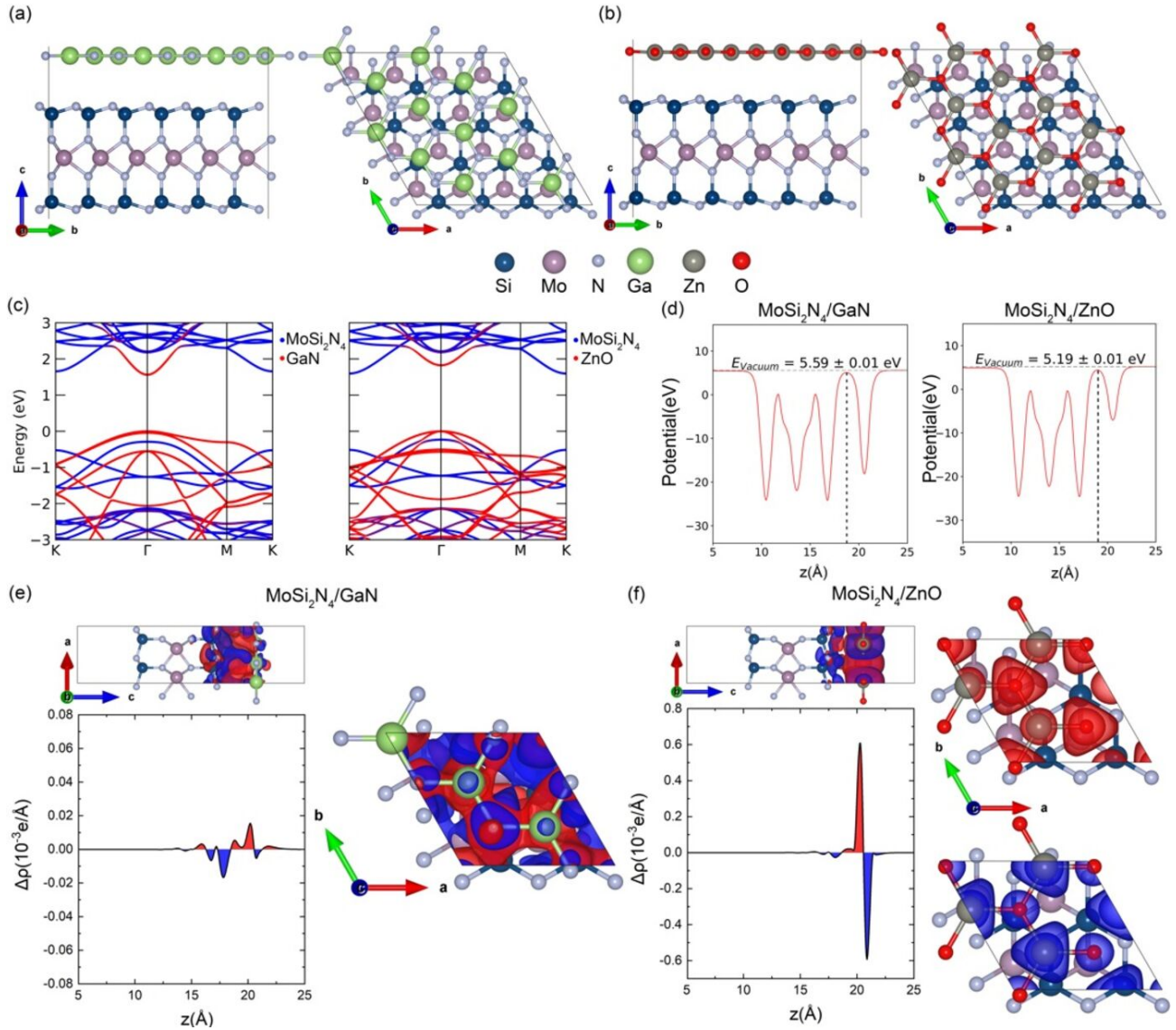


FIG. 1. (a) Top and side view of MoSi₂N₄/GaN (b) Top and side view of MoSi₂N₄/ZnO. (c) Band structures of MoSi₂N₄/GaN and MoSi₂N₄/ZnO. (d) Potential plots of MoSi₂N₄/GaN and MoSi₂N₄/ZnO, with the black dotted line showing heterostructure interface. (e) Left hand side, charge density difference plots showing cross section isosurface and charge density difference in the of MoSi₂N₄/GaN, red and blue showing charge accumulation and depletion respectively. Right hand side, isosurface of charge density difference from the top (f) Left hand side, charge density difference plots showing cross section isosurface and charge density difference of MoSi₂N₄/ZnO. Right hand side, isosurface of charge density difference from the top

a non-layered, non-exfoliatable compound. Thus, ongoing research dominantly focuses on the growth of high-quality GaN monolayers [24, 40]. Nevertheless, novel applications, such as flexible electronics [41], light-emitting diodes [42] and piezoelectric strain-gated logic gates [43], have been demonstrated recently, thus suggesting the potential of 2D GaN in electronics and optoelectronics applications. Beyond GaN, other 2D WBG semiconductors, such as GaSe, GaS and SnS₂, have been also fabricated. These monolayers exhibit fast response times and high photoresponsivity [44, 45], good compatibility in flexible device applications [45], and can be incorporated for logic gates applications with large on-off ratios

[46].

Motivated by the potentials of MA₂Z₄ based WBG semiconductors, we perform first-principle calculations on the electronic and structural properties of MoSi₂N₄/GaN and MoSi₂N₄/ZnO VDWs by using density functional theory (DFT). We find that MoSi₂N₄/GaN and MoSi₂N₄/ZnO are Type-I direct band gap and Type-II indirect band gap VDWs, respectively. Interestingly, an external electric fields perpendicular to the plane of the VDWs can be used to drive a transition between direct and indirect band gaps, thus indicating a field-effect tunable optoelectronic properties of

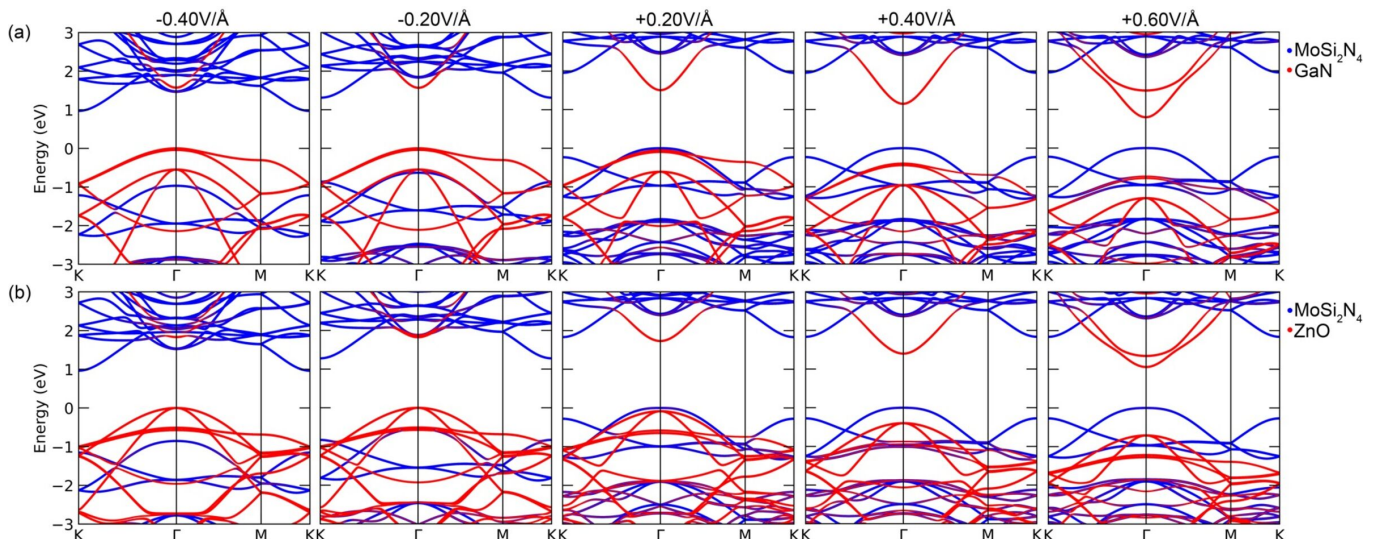


FIG. 2. (a) Band structure of $\text{MoSi}_2\text{N}_4/\text{GaN}$ when subjected to external electric fields, with corresponding external electric field values at the top. (b) Band structure of $\text{MoSi}_2\text{N}_4/\text{ZnO}$ when subjected to external electric fields, with corresponding external electric field values at the top.

$\text{MoSi}_2\text{N}_4/\text{GaN}$ and $\text{MoSi}_2\text{N}_4/\text{ZnO}$ VDWHs. Additionally, the electronic properties, band alignment and the direct/indirect band gap nature of $\text{MoSi}_2\text{N}_4/\text{GaN}$ and $\text{MoSi}_2\text{N}_4/\text{ZnO}$ can be further controlled under mechanical compression and strain. These results suggest the potentials of $\text{MoSi}_2\text{N}_4/\text{WBG}$ -2D-semiconductor VDWHs as a versatile material platform for tunable electronic and optoelectronic device applications.

All simulations are carried out using DFT implemented in the Vienna *Ab initio* Simulation Package [47–50]. PAW pseudopotentials [51] are used to simulate the ion electron bonding and the layers are relaxed using GGA PBE [52] with Grimme DFT-D3 vdW [53] interactions between the monolayers. It is known that PBE underestimates the band gaps and that HSE06 will produce better band gaps for 2D GaN and ZnO [24, 54]. Using PBE allows the effect of strain and external electric fields to be studied without the high computational costs of HSE06 and has been used before in previous literature [55, 56], so PBE results are used and presented here. Crucially, the general trend of the band structure and band alignment are expected to be sufficiently captured by PBE. We thus expect our key findings to be qualitatively accurate using PBE calculations. All materials were sampled using a gamma-centred Brillouin zone at $11 \times 11 \times 1$ using the Monkhorst-Pack grid [57]. Ionic force convergence was set to 0.01 V/Å and electronic convergence was set to 10^{-8} eV. A vacuum layer of 20 Å was used to prevent interactions between periodic layers. The energy cutoff at 500 eV was made to allow comparisons between materials and different electric field and strain settings. Dipole corrections are enabled in all calculations for consistency. Spin orbit coupling was not considered in this paper, since MoSi_2N_4 [12], GaN and ZnO are non-magnetic semiconductors. Thus, spin is unlikely to play

a major role in the properties of the studied VDWH, with spin-orbit coupling showing only small differences [58–61]. However, we note that the magnetic properties of VDWH can be altered by means of doping [62], hydrogen adsorption [63] or proximity effects to magnetic materials [64], thus suggesting further avenues for magnetic and spintronic properties engineering of MoSi_2N_4 -based VDWH.

MoSi_2N_4 , GaN and ZnO layers are constructed using previously reported experimental and computational lattice parameters [12, 17, 24, 28]. The bond lengths of the fully relaxed monolayers are 2.087 Å for Mo-N, 1.858 Å for Ga-N and 1.906 Å for Zn-O, which are in agreement with those previously reported. Several stacking configurations were built using QuantumATK, with strain distributed among the GaN and ZnO layer. The binding energy is calculated as follows: $E_b = (E_{vdW} - E_{\text{MoSi}_2\text{N}_4} - E_\mu)/34$, where μ is GaN or ZnO. The binding energy of all configurations was found to be negative, suggesting their energetic stability. The binding energy was all VDWHs very similar to within 0.0001 eV per atom, hence the slightly lower energy was chosen. The final stacking configuration has a binding energy of -0.0158 eV/atom for $\text{MoSi}_2\text{N}_4/\text{GaN}$ and -0.0202 eV/atom for $\text{MoSi}_2\text{N}_4/\text{ZnO}$. The overall lattice strain for $\text{MoSi}_2\text{N}_4/\text{GaN}$ is 2.68 % and 0.92 % for $\text{MoSi}_2\text{N}_4/\text{ZnO}$.

The chosen VDWHs consist of 2×2 unit cells of MoSi_2N_4 and $\sqrt{3} \times \sqrt{3}$ unit cells of GaN or ZnO. The 2×2 supercells are shown in Figs. 1(a) and (b). The fully relaxed $\text{MoSi}_2\text{N}_4/\text{GaN}$ and $\text{MoSi}_2\text{N}_4/\text{ZnO}$ have an interlayer distance of 3.44 Å and 3.15 Å, respectively, which are well above the vdW radius of 2.05 Å (gallium) [65], 1.55 Å (nitrogen) [65] and 1.52 Å (oxygen) [65]. The electronic band structures of the isolated MoSi_2N_4 , GaN and ZnO monolayers exhibit the band gaps of 1.796 eV,

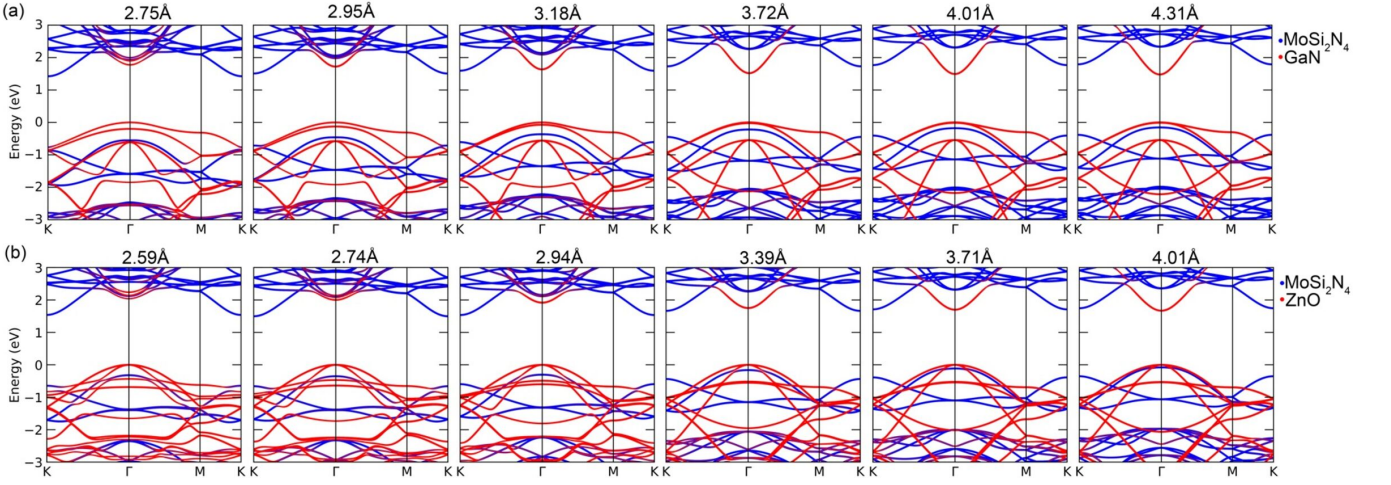


FIG. 3. (a) Band structure of $\text{MoSi}_2\text{N}_4/\text{GaN}$, with corresponding interlayer distance at the top. (b) Band structure of $\text{MoSi}_2\text{N}_4/\text{ZnO}$, with corresponding interlayer distance at the top

2.118 eV, and 1.648 eV, respectively. The work function is calculated for the monolayers and VDWs as $W = E_{\text{vacuum}} - E_{\text{Fermi}}$, where E_{vacuum} is the vacuum energy and E_{Fermi} is the Fermi level. The calculated E_{vacuum} are 4.6 eV, 0.91 eV and 0.54 eV for MoSi_2N_4 , GaN and ZnO respectively. Correspondingly, the work functions of MoSi_2N_4 , GaN and ZnO are calculated as 5.25 eV, 5.23 eV and 5.36 eV, respectively.

The electronic band structures of the modified monolayers based on the structural parameters taken from the VDWs are plotted in Supplementary Materials Figure S1. Compared to the free-standing monolayers, the band gaps are modified to 1.952 eV, 1.482 eV and 1.648 eV for MoSi_2N_4 , GaN and ZnO, respectively. The overall MoSi_2N_4 , GaN and ZnO band structures are preserved in forming the VDWs. However, the conduction band of GaN and ZnO at Γ is split from a single continuous band into avoided crossings across multiple MoSi_2N_4 conduction bands. The $\text{MoSi}_2\text{N}_4/\text{GaN}$ has a Type-I direct band gap of 1.56 eV at Γ -point, with both VBM and CBM contributed by the GaN. In contrast, $\text{MoSi}_2\text{N}_4/\text{ZnO}$ has a Type-II indirect band gap of 1.60 eV between the VBM at the Γ -point as contributed by ZnO, and the CBM at the K -point as contributed by MoSi_2N_4 CBM.

We now examine the electron transfer in Figs. 1(e) and 1(f) for $\text{MoSi}_2\text{N}_4/\text{GaN}$ and $\text{MoSi}_2\text{N}_4/\text{ZnO}$, respectively. In general, $\text{MoSi}_2\text{N}_4/\text{GaN}$ has a nett transfer of electrons from MoSi_2N_4 to GaN, while $\text{MoSi}_2\text{N}_4/\text{ZnO}$ has a nett transfer of electrons in the opposite direction from ZnO towards MoSi_2N_4 . In Fig. 1(e), the electron distributions of the $\text{MoSi}_2\text{N}_4/\text{GaN}$ are shown at the cross-sectional and the top views. The electrons accumulate at the contact interface and generally spread out along the interface. In contrast, the electron charge accumulation and depletion in concentric shells around each atom in ZnO for the $\text{MoSi}_2\text{N}_4/\text{ZnO}$ as shown in Fig. 1(f). The differential charge charge densities are calculated via $\Delta\rho = \rho_{\text{vdw}} - \rho_{\text{MoSi}_2\text{N}_4} - \rho_{\mu}$, where μ is GaN or ZnO,

ρ_{vdw} is the charge density of the VDWH and ρ_{μ} is the charge density of the individual monolayer. Comparing the differential charge density plots in Figs. 1(e) and (f), it is seen that the peak magnitude of the charge transfer in $\text{MoSi}_2\text{N}_4/\text{GaN}$ is 40 times smaller than that of $\text{MoSi}_2\text{N}_4/\text{ZnO}$, due to the smaller work function difference between GaN and MoSi_2N_4 versus that of ZnO and MoSi_2N_4 . The sharp peaks in the differential charge density plot also reveals a significant electron redistribution within the ZnO monolayer but not the MoSi_2N_4 , which is in strong contrast to the case of $\text{MoSi}_2\text{N}_4/\text{ZnO}$ VDWH where the electron distributions occur with comparable strength in both MoSi_2N_4 and GaN.

We next examine the heterostructures response to external electric fields. An external electric field was added in a self-consistent manner on relaxed heterostructures in steps of $0.2\text{V}/\text{\AA}$ in Fig. 2. To illustrate the effect of an external electric field on the VDWs, the differences in charge density are calculated as: $\Delta\rho(E) = \rho(E) - \rho_{\text{initial}}$ where E is the external electric field, $\rho(E)$ and ρ_{initial} are the charge density of the VDWs with and without electric field, respectively. The external electric field induces electron depletion on GaN or ZnO, and electron accumulation on MoSi_2N_4 due to the electrostatic-induced charge redistributions (see Supplementary Materials for the charge density difference and plane-averaged electrostatic potential plots). Thus, at increasing positive electric field the energy of MoSi_2N_4 bands are raised relative to GaN and ZnO, while the GaN and ZnO bands are lowered relative to MoSi_2N_4 [see Figs. 2(a) and 2(b) for $\text{MoSi}_2\text{N}_4/\text{GaN}$ and $\text{MoSi}_2\text{N}_4/\text{ZnO}$, respectively]. Correspondingly, the CBM of both GaN and ZnO at the Γ -point decreases in energy. Both VDWs thus undergo a transformation into the Type-II direct band gap VDWs, featuring the CBM from GaN and ZnO and VBM from MoSi_2N_4 .

Under a negative electric field, electron accumulation is induced on GaN and ZnO heterostructure interface and

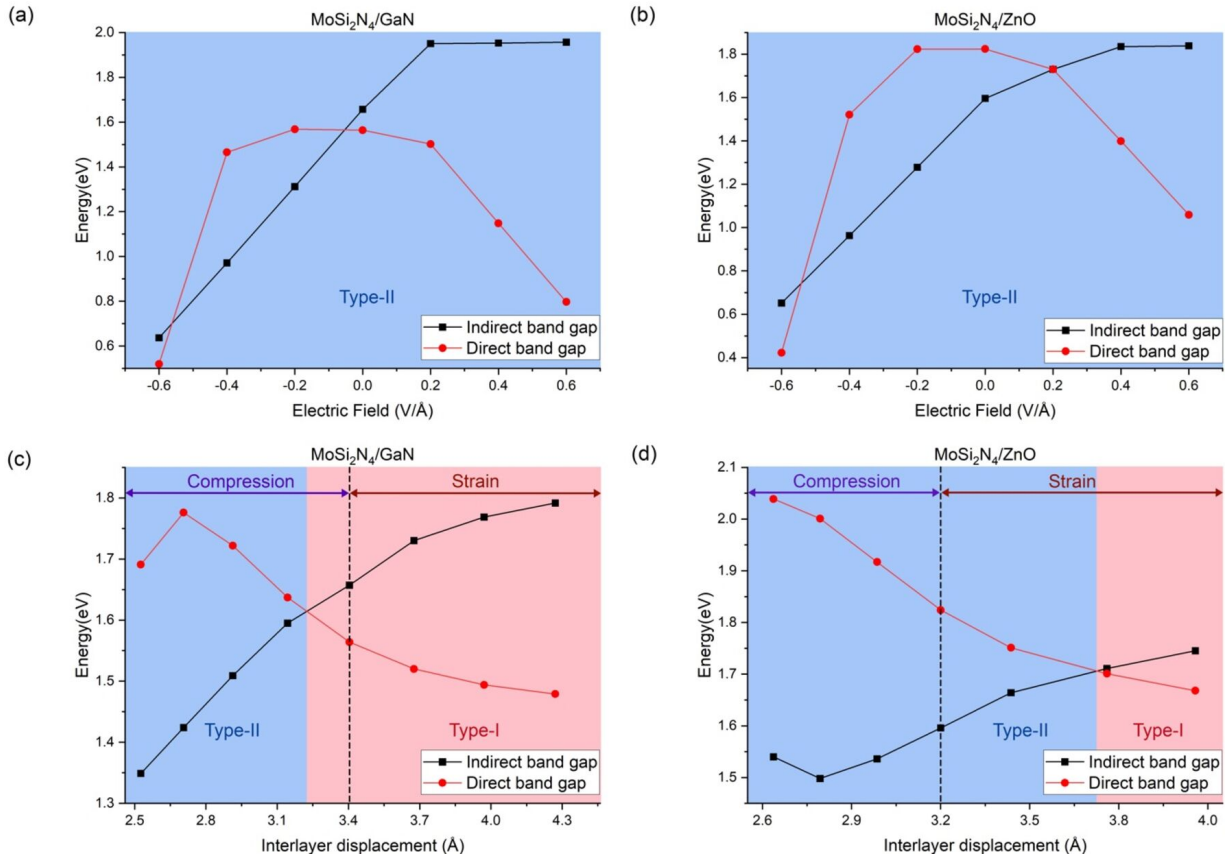


FIG. 4. (a) Band gap plots of MoSi₂N₄/GaN under external electric field. (b) Band gap plots of MoSi₂N₄/ZnO under external electric field. (c) Band gap plots of MoSi₂N₄/GaN under strain and compression. (d) Band gap plots of MoSi₂N₄/ZnO under strain and compression

depleted on MoSi₂N₄. In this case, the GaN and ZnO energy is raised relative to MoSi₂N₄, shifting the band structure of GaN and ZnO upwards generally. This results in the CBM of MoSi₂N₄ at *K*-point being lower in energy than the Γ -point CBM of GaN and ZnO, turning both VDWHs into an indirect band gap Type-II VDWHs [see Figs. 2(a) and 2(b) for MoSi₂N₄/GaN and MoSi₂N₄/ZnO, respectively].

Experimentally, the interlayer distance can be tuned by several methods during material fabrication stage, such as insertion of hBN buffer layer [66] or via nanomechanical pressure [67]. We thus investigate how mechanical strain or compression applied perpendicularly to the VDWHs influences the electronic band structures by changing the interlayer spacing in steps of 0.3 Å. [see Figs. 3(a) and 3(b) for MoSi₂N₄/GaN and MoSi₂N₄/ZnO, respectively]. For compression, we decrease the bond lengths of Mo-N from 2.080Å and 2.088Å from the initial MoSi₂N₄/GaN and MoSi₂N₄/ZnO VDWHs, respectively, to 2.062Å and 2.068Å in MoSi₂N₄/GaN and MoSi₂N₄/ZnO VDWHs, respectively. When the VDWHs are compressed [see Figs. 3(a) and (b)], MoSi₂N₄ is observed to decrease in energy with respect to GaN and ZnO in general. These

changes are similar to those observed when the VDWHs are subject to an external electric field in the positive *z*-direction. Furthermore, the width of the vacuum tunneling potential barrier between the monolayers decreases under compression (see the plane-averaged electrostatic potential profile plots in the SM), which leads to easier tunneling of electrons from GaN and ZnO to MoSi₂N₄. The GaN or ZnO sublayer increases in energy with increasing compression, with bands shifting higher relative to MoSi₂N₄. For MoSi₂N₄/GaN, the CBM of GaN at the Γ -point retracts into the higher energies, resulting in the transformation from direct band gap Type-I into indirect band gap Type-II band alignment. For MoSi₂N₄/ZnO, an indirect band gap Type-II band alignment is similarly observed at large compression.

For tensile strain, the bond lengths of Mo-N increases from 2.080Å and 2.088Å in initial MoSi₂N₄/GaN and MoSi₂N₄/ZnO VDWH to 2.083Å and 2.090Å in the strained VDWHs at maximum strain. GaN and ZnO is observed to decrease in energy with the band structure shifting downwards relative to MoSi₂N₄. However, the increasing width of the potential barrier between the monolayers as the interlayer distance is increased (see SM) severely limits the ability of electrons

to tunnel across and reduces the coupling between the two materials. Thus, the changes in the band structure less dramatic as compared to the case of compression. For MoSi₂N₄/GaN, the band structure remains a direct band gap Type-I band alignment under increasing strain with decreasing change in direct band gap energy. For MoSi₂N₄/ZnO, the band structure changes from indirect band gap Type-II to direct band gap Type-I band alignment as the ZnO CBM energy decreases relative to MoSi₂N₄ CBM.

The properties of the band gap and the heterostructure types are summarized in Fig. 4, with blue-shaded regions representing Type-II alignment and red-shaded regions representing Type-I alignment. The VDWHs retain the Type-II band alignment under external electric fields in both directions as shown in Figs. 4(a) and 4(b) for MoSi₂N₄/GaN and MoSi₂N₄/ZnO, respectively. However, the heterostructures changes between direct and indirect band gap when the electric fields are varied in the range of 0.0 V/Å to -0.6 V/Å for MoSi₂N₄/GaN and +0.2V/Å to -0.6 V/Å for MoSi₂N₄/ZnO. This is in contrasts to the case of compression and strain, as shown in Figs. 4(c) and 4(d) for MoSi₂N₄/GaN and MoSi₂N₄/ZnO, respectively. Under compression, MoSi₂N₄/GaN changes from direct band gap Type-I to indirect band gap Type-II band alignment, while MoSi₂N₄/ZnO changes from indirect band gap Type-I to indirect band gap Type-II band alignments. Under strain, MoSi₂N₄/GaN remains unchanged while MoSi₂N₄/ZnO changes from Type-I indirect band gap to Type-I direct band gap under strain.

In summary, the electronic properties of MoSi₂N₄-based wide band gap semiconductor van der Waals heterostructures are studied using density functional theory simulations. The MoSi₂N₄/GaN and MoSi₂N₄/ZnO heterostructures are in direct band gap Type-I and indirect band gap Type-II band alignment, respectively. Differential charge density analysis suggests that the electron redistribution upon forming the contact heterostructure is much stronger in MoSi₂N₄/ZnO than that in MoSi₂N₄/GaN. Furthermore, we show that the application of an external perpendicular electric field or mechanical strain effectively alter the band gap type and the band alignment type of the heterostructures, thus offering a tuning knob for engineering the electronic and optoelectronic properties of the heterostructures. These find-

ings reveal the potentials of MoSi₂N₄-based wide band gap van der Waals heterostructures as a versatile platform for designing novel tunable optoelectronics.

SUPPLEMENTARY MATERIAL

See supplementary material for the electronic band structures of isolated monolayers, and the plane-averaged differential charge and electrostatic potential profiles of the MoSi₂N₄/ZnO and MoSi₂N₄/GaN heterostructures.

ACKNOWLEDGMENTS

This work is supported by A*STAR AME IRG (A2083c0057) and Singapore University of Technology and Design Start-Up Research grant (Project No. SRG SCI 2021 163). J.Q.N. acknowledge the PhD Scholarship support from the Singapore University of Technology and Design. The calculations were carried out using the computational resources provided by the Titan supercomputing facility in SUTD and the National Supercomputing Centre (NSCC) Singapore.

AUTHOR DECLARATIONS

Conflict of Interest

The authors declare that there are no conflicts of interest.

Author Contributions

J.Q.N. performed the simulations and data analysis. Q.W., L.K.A. and Y.S.A. supervised the project. All authors contributed to the writing and the revision to this work.

DATA AVAILABILITY

The data that support the findings of this study are available from the corresponding author upon reasonable request.

-
- [1] Y. Liu, N. O. Weiss, X. Duan, H.-C. Cheng, Y. Huang, and X. Duan, *Nat. Rev. Mater.* **1**, 1 (2016).
 - [2] V. Vaño, M. Amini, S. C. Ganguli, G. Chen, J. L. Lado, S. Kezilebieke, and P. Liljeroth, arXiv:2103.11989 (2021).
 - [3] X. Liu, K. Watanabe, T. Taniguchi, B. I. Halperin, and P. Kim, *Nat. Phys.* **13**, 746 (2017).
 - [4] L. Cao, G. Zhou, Q. Wang, L. Ang, and Y. S. Ang, *Appl. Phys. Lett.* **118**, 013106 (2021).
 - [5] L. Cao, G. Zhou, Q. Wu, S. A. Yang, H. Y. Yang, Y. S. Ang, and L. Ang, *Phys. Rev. Appl.* **13**, 054030 (2020).
 - [6] Y. Liu, J. Guo, E. Zhu, L. Liao, S.-J. Lee, M. Ding, I. Shaker, V. Gambin, Y. Huang, and X. Duan, *Nature* **557**, 696 (2018).
 - [7] Y. Liu, P. Stradins, and S.-H. Wei, *Sci. Adv.* **2**, e1600069 (2016).
 - [8] S. Hofstein and G. Warfield, *IEEE Transactions on Electron Devices* **12**, 66 (1965).

- [9] S. O. Koswatta, M. S. Lundstrom, and D. E. Nikonov, IEEE Transactions on Electron Devices **56**, 456 (2009).
- [10] X. Gan, R.-J. Shiue, Y. Gao, I. Meric, T. F. Heinz, K. Shepard, J. Hone, S. Assefa, and D. Englund, Nature photonics **7**, 883 (2013).
- [11] W. Yu, S. Li, Y. Zhang, W. Ma, T. Sun, J. Yuan, K. Fu, and Q. Bao, Small **13**, 1700268 (2017).
- [12] Y.-L. Hong, Z. Liu, L. Wang, T. Zhou, W. Ma, C. Xu, S. Feng, L. Chen, M.-L. Chen, D.-M. Sun, et al., Science **369**, 670 (2020).
- [13] Q. Wang, L. Cao, S.-J. Liang, W. Wu, G. Wang, C. H. Lee, W. L. Ong, H. Y. Yang, L. K. Ang, S. A. Yang, et al., NPJ 2D Mater. Appl. **5**, 71 (2021).
- [14] H. Zhao, G. Yang, Y. Liu, X. Yang, Y. Gu, C. Wei, Z. Xie, Q. Zhang, B. Bian, X. Zhang, et al., ACS Appl. Electron. Mater. **3**, 5086 (2021).
- [15] X. Sun, Z. Song, N. Huo, S. Liu, C. Yang, J. Yang, W. Wang, and J. Lu, J. Mater. Chem. C **9**, 14683 (2021).
- [16] K. Nandan, B. Ghosh, A. Agarwal, S. Bhowmick, and Y. S. Chauhan, IEEE T. Electron. Dev. (2021).
- [17] A. Ray, S. Tyagi, N. Singh, and U. Schwingschlog, ACS omega (2021).
- [18] C.-c. Jian, X. Ma, J. Zhang, and X. Yong, J. Phys. Chem. C **125**, 15185 (2021).
- [19] X. Cai, Z. Zhang, Y. Zhu, L. Lin, W. Yu, Q. Wang, X. Yang, X. Jia, and Y. Jia, J. Mater. Chem. C **9**, 10073 (2021).
- [20] A. Bafekry, M. Faraji, A. A. Ziabari, M. Fadlallah, C. V. Nguyen, M. Ghergherehchi, and S. Feghhi, New J. Chem. **45**, 8291 (2021).
- [21] C. Nguyen, N. V. Hoang, H. V. Phuc, A. Y. Sin, and C. V. Nguyen, J. Phys. Chem. Lett. **12**, 5076 (2021).
- [22] J. Zhao, X. Jin, H. Zeng, C. Yao, and G. Yan, Appl. Phys. Lett. **119**, 213101 (2021).
- [23] Q. Wu, L. Cao, Y. S. Ang, and L. K. Ang, Appl. Phys. Lett. **118**, 113102 (2021).
- [24] Z. Y. Al Balushi, K. Wang, R. K. Ghosh, R. A. Vilá, S. M. Eichfeld, J. D. Caldwell, X. Qin, Y.-C. Lin, P. A. DeSario, G. Stone, et al., Nat. Mater. **15**, 1166 (2016).
- [25] J. Lee, D. C. Sorescu, and X. Deng, J. Phys. Chem. Lett. **7**, 1335 (2016).
- [26] X. Rong, X. Wang, S. V. Ivanov, X. Jiang, G. Chen, P. Wang, W. Wang, C. He, T. Wang, T. Schulz, et al., Adv. Mater. **28**, 7978 (2016).
- [27] J. Tian, L. Liu, S. Xia, Y. Diao, and F. Lu, Opt. Commun. **454**, 124498 (2020).
- [28] J. Ben, X. Liu, C. Wang, Y. Zhang, Z. Shi, Y. Jia, S. Zhang, H. Zhang, W. Yu, D. Li, et al., Adv. Mater. p. 2006761 (2021).
- [29] A. Mahmud, A. A. Khan, P. Voss, T. Das, E. Abdel-Rahman, and D. Ban, Adv. Mater. Interfaces **5**, 1801167 (2018).
- [30] B. Wang, J. Ning, J. Zhang, D. Wang, X. Yang, Y. Jia, C. Zhang, Y. Zeng, and Y. Hao, Applied Physics Letters **119**, 163504 (2021).
- [31] A. Yoshikawa, H. Matsunami, and Y. Nanishi, in *Wide bandgap semiconductors* (Springer, 2007), pp. 1–24.
- [32] H. Yuan, J. Su, P. Zhang, Z. Lin, J. Zhang, J. Zhang, J. Chang, and Y. Hao, Materials Today Physics **21**, 100549 (2021), ISSN 2542-5293.
- [33] A. A. Fletcher and D. Nirmal, Superlattices Microstruct. **109**, 519 (2017).
- [34] W. Zhang, X. Huang, Z. Liu, F. C. Lee, S. She, W. Du, and Q. Li, IEEE T. Power. Electr. **31**, 1344 (2015).
- [35] X. Ding, Y. Zhou, and J. Cheng, CES Transactions on Electrical Machines and Systems **3**, 54 (2019).
- [36] C. Jagadish and S. J. Pearton, *Zinc oxide bulk, thin films and nanostructures: processing, properties, and applications* (Elsevier, 2011).
- [37] H.-K. Hong, J. Jo, D. Hwang, J. Lee, N. Y. Kim, S. Son, J. H. Kim, M.-J. Jin, Y. C. Jun, R. Erni, et al., Nano letters **17**, 120 (2017).
- [38] R. Gang, L. Xu, Y. Xia, L. Zhang, S. Wang, and R. Li, ACS omega **6**, 3831 (2021).
- [39] N. Al-Hardan, M. Abdullah, N. Ahmed, F. Yam, and A. A. Aziz, Superlattices and Microstructures **51**, 765 (2012).
- [40] Y. Chen, K. Liu, J. Liu, T. Lv, B. Wei, T. Zhang, M. Zeng, Z. Wang, and L. Fu, Journal of the American Chemical Society **140**, 16392 (2018).
- [41] N. R. Glavin, K. D. Chabak, E. R. Heller, E. A. Moore, T. A. Prusnick, B. Maruyama, D. E. Walker Jr, D. L. Dorsey, Q. Paduano, and M. Snure, Advanced Materials **29**, 1701838 (2017).
- [42] K. Chung, C.-H. Lee, and G.-C. Yi, Science **330**, 655 (2010).
- [43] R. Yu, W. Wu, Y. Ding, and Z. L. Wang, ACS nano **7**, 6403 (2013).
- [44] P. Hu, Z. Wen, L. Wang, P. Tan, and K. Xiao, ACS nano **6**, 5988 (2012).
- [45] P. Hu, L. Wang, M. Yoon, J. Zhang, W. Feng, X. Wang, Z. Wen, J. C. Idrobo, Y. Miyamoto, D. B. Geohegan, et al., Nano letters **13**, 1649 (2013).
- [46] H. Song, S. Li, L. Gao, Y. Xu, K. Ueno, J. Tang, Y. Cheng, and K. Tsukagoshi, Nanoscale **5**, 9666 (2013).
- [47] G. Kresse and J. Hafner, Phys. Rev. B **47**, 558 (1993).
- [48] G. Kresse and J. Hafner, Phys. Rev. B **49**, 14251 (1994).
- [49] G. Kresse and J. Furthmüller, Comput. Mater. Sci. **6**, 15 (1996).
- [50] G. Kresse and J. Furthmüller, Phys. Rev. B **54**, 11169 (1996).
- [51] G. Kresse and D. Joubert, Phys. Rev. B **59**, 1758 (1999).
- [52] J. P. Perdew, K. Burke, and M. Ernzerhof, Phys. Rev. Lett. **77**, 3865 (1996).
- [53] S. Grimme, J. Antony, S. Ehrlich, and H. Krieg, J. Chem. Phys. **132**, 154104 (2010).
- [54] C. Supatutkul, S. Pramchu, A. Jaroenjittichai, and Y. Laosiritaworn, in *J. Phys. Conf. Ser.* (IOP Publishing, 2017), vol. 901, p. 012172.
- [55] X. Chen, H. Sheng, J. Wang, G. Tang, J. Zhang, and D. Bai, Vacuum **174**, 109232 (2020).
- [56] L. Huang, Q. Yue, J. Kang, Y. Li, and J. Li, Journal of Physics: Condensed Matter **26**, 295304 (2014).
- [57] H. J. Monkhorst and J. D. Pack, Phys. Rev. B **13**, 5188 (1976).
- [58] A. Onen, D. Kecik, E. Durgun, and S. Ciraci, Physical Review B **93**, 085431 (2016).
- [59] J. M. Kasper, D. R. Gamelin, and X. Li, The Journal of Chemical Physics **152**, 014308 (2020).
- [60] F. S. Saoud, J. C. Plenet, and M. Henini, Journal of Alloys and Compounds **619**, 812 (2015).
- [61] R. Islam, B. Ghosh, C. Autieri, S. Chowdhury, A. Bansil, A. Agarwal, and B. Singh, Physical Review B **104**, L201112 (2021).
- [62] Q. Zhao, Z. Xiong, Z. Qin, L. Chen, N. Wu, and X. Li, Journal of Physics and Chemistry of Solids **91**, 1 (2016).
- [63] R. González-Ariza, O. Martínez-Castro, M. G. Moreno-Armenta, A. Gonzalez-Garcia, W. Lopez-Perez, and

- R. Gonzalez-Hernandez, *Physica B: Condensed Matter* **569**, 57 (2019).
- [64] Q. Wu and L. K. Ang, *Applied Physics Letters* **120**, 022401 (2022).
- [65] S. S. Batsanov, *Inorg. Mater.* **37**, 871 (2001).
- [66] H. Fang, C. Battaglia, C. Carraro, S. Nemsak, B. Ozdol, J. S. Kang, H. A. Bechtel, S. B. Desai, F. Kronast, A. A. Unal, et al., *Proceedings of the National Academy of Sciences* **111**, 6198 (2014).
- [67] M. Dienwiebel, G. S. Verhoeven, N. Pradeep, J. W. Frenken, J. A. Heimberg, and H. W. Zandbergen, *Physical review letters* **92**, 126101 (2004).